The Company of
Biologists

RESEARCH ARTICLE

Diversity in cell motility reveals the dynamic nature of the formation of zebrafish taste sensory organs

Marina Soulika[1], Anna-Lila Kaushik[1,§], Benjamin Mathieu[1,§], Raquel Lourenço[1,‡,¶], Anna Z. Komisarczuk[2,*,¶], Sebastian Alejo Romano[1], Adrien Jouary[1], Alicia Lardennois[1], Nicolas Tissot[3], Shinji Okada[4], Keiko Abe[4], Thomas S. Becker[2] and Marika Kapsimali[1,**]

ABSTRACT

Taste buds are sensory organs in jawed vertebrates, composed of distinct cell types that detect and transduce specific taste qualities. Taste bud cells differentiate from oropharyngeal epithelial progenitors, which are localized mainly in proximity to the forming organs. Despite recent progress in elucidating the molecular interactions required for taste bud cell development and function, the cell behavior underlying the organ assembly is poorly defined. Here, we used time-lapse imaging to observe the formation of taste buds in live zebrafish larvae. We found that *tg(fgf8a.dr17)*-expressing cells form taste buds and get rearranged within the forming organs. In addition, differentiating cells move from the epithelium to the forming organs and can be displaced between developing organs. During organ formation, *tg(fgf8a.dr17)* and type II taste bud cells are displaced in random, directed or confined mode relative to the taste bud they join or by which they are maintained. Finally, *ascl1a* activity in the 5-HT/type III cell is required to direct and maintain *tg(fgf8a.dr17)*-expressing cells into the taste bud. We propose that diversity in displacement modes of differentiating cells acts as a key mechanism for the highly dynamic process of taste bud assembly.

KEY WORDS: Taste bud, Time-lapse, Ascl1a, fgf8a, Taste receptor cell, MSD

INTRODUCTION

Taste buds are vertebrate sensory organs responding to taste stimuli, composed of three major differentiated cell types: type I (support), type II (taste receptor) and type III (presynaptic) cells, which express specific molecules to detect and transduce salty, bitter, sweet, umami, sour or carbonated taste (Chandrashekar et al., 2006, 2009; Chaudhari and Roper, 2010; Yarmolinsky et al., 2009). In contrast to other sensory organs with a specific number of cells (i.e. insect ommatidia; Wernet et al., 2015), the cellular organization of taste buds is variable within a single species; an adult mouse taste bud contains 50-100 cells of types I, II or III

[1]IBENS, Ecole Normale Supérieure, CNRS UMR8197, INSERM U1024, 75230 Paris, France. [2]Developmental Neurobiology and Genomics, Brain and Mind Research Institute, University of Sydney, Camperdown, NSW 2050, Australia. [3]Institut Jacques Monod, CNRS UMR7592, University Paris Diderot, 75013 Paris, France. [4]Department of Applied Biological Chemistry, Graduate School of Agricultural and Life Sciences, The University of Tokyo, Tokyo 113-8657, Japan.
*Present address: Sea Lice Research Centre, Department of Biology, University of Bergen, 5020 Bergen, Norway. ‡Present address: CEDOC, NOVA Medical School, NOVA University of Lisbon, 1169-056 Lisbon, Portugal.
§These authors contributed equally to this work
¶These authors contributed equally to this work

**Author for correspondence (marika.kapsimali@ens.fr)

M.K., 0000-0001-9327-5166

but their proportion varies among taste bud loci (i.e. Ohtubo and Yoshii, 2011).

Upon stimulation, taste bud cells, which are dedicated to specific taste qualities, release transmitters (Chaudhari and Roper, 2010; Roper, 2013), including ATP (Finger et al., 2005; Taruno et al., 2013) that bind to their corresponding receptors (Huang et al., 2011b; Kinnamon and Finger, 2013) and transmit information to sensory afferent fibers (Barretto et al., 2015; Vandenbeuch et al., 2015). Taste bud cells communicate with each other [i.e. via 5-hydroxytryptamine (5-HT)] to locally ensure appropriate signal amplification/attenuation (Dvoryanchikov et al., 2011; Huang et al., 2009, 2011a; Roper, 2013).

In jawed vertebrates, taste bud cells derive from progenitors located within the oropharyngeal epithelium that has ectodermal or endodermal origin (Barlow and Northcutt, 1995, 1997; Kapsimali and Barlow, 2013; Kapsimali et al., 2011; Liu et al., 2012; Okubo et al., 2009; Rothova et al., 2012; Stone et al., 2002; Thirumangalathu et al., 2009). In developing mice, Shh-expressing precursors generate transient taste bud cells in focal thickenings of the lingual epithelium, known as taste placodes (Thirumangalathu et al., 2009). However, dividing cells that generate taste bud cells are mostly but not exclusively located within the epithelium in proximity to, rather than within, taste buds (Nguyen et al., 2012; Okubo et al., 2009; Perea-Martinez et al., 2013; Yee et al., 2013). Progenitors expressing keratin 15 and keratin 14 give rise to taste bud cells and keratinocytes (Okubo et al., 2009). In the adult posterior tongue, Lgr5/6-expressing progenitors generate all taste bud cell types *ex vivo* (Aihara et al., 2015; Ren et al., 2014; Yee et al., 2013). Fate-mapping and thymidine-analogue tracing assays have suggested that newly forming cells are translocated from the epithelium to the taste bud, but the process of displacement remains unclear (Barlow and Northcutt, 1995; Liu et al., 2012; Nguyen et al., 2012; Okubo et al., 2009; Perea-Martinez et al., 2013; Stone et al., 2002; Thirumangalathu et al., 2009; Yee et al., 2013). This could be done passively; newborn cells could intermingle, be randomly displaced in the limited space and reach the organ; alternatively, cells could migrate towards forming organs. The differentiation of taste bud cells from precursors located inside and outside the organ, cell translocation from the epithelium to the organ and variability in the cell composition of these organs, all raise the issue of displacement behavior of one cell relative to another that results in taste bud assembly.

Wnt/β-catenin, Bmp, Fgf and Shh proteins are required for initial specification and patterning of taste bud placodes (Beites et al., 2009; Iwatsuki et al., 2007; Liu et al., 2007, 2013; Mistretta et al., 2003; Miura et al., 2014; Petersen et al., 2011; Zhou et al., 2006). For instance, balanced Fgf10 and Sprouty1/2 (Spry1/2) signaling defines the progenitor cell territory that generates appropriate

DEVELOPMENT

number of circumvallate taste buds (Petersen et al., 2011). Differentiation of distinct cell types relies on miR-200, Ascl1/ Notch1/Hes1, Skn-1a (Pou2f3) and β-catenin (Ctnnb1) activity (Gaillard et al., 2015; Kapsimali et al., 2011; Matsumoto et al., 2011; Ota et al., 2009; Seta et al., 2011). In particular, Ascl1a is required for 5-HT synthesis in differentiating type III cells in mice and zebrafish (Kapsimali et al., 2011; Seta et al., 2011). Shh inhibits Wnt/β-catenin signaling (Iwatsuki et al., 2007) and Notch1 activity restores the number of type II cells in zebrafish larvae with compromised Fgf receptor signaling (Kapsimali et al., 2011), indicating that epistatic interactions among these and other signaling pathways regulate the transition from progenitor to differentiated taste bud cells (Barlow and Klein, 2015; Kapsimali and Barlow, 2013; Kist et al., 2014).

Despite recent progress in elucidating the molecular mechanisms of taste bud development and physiology, the cell behavior that underlies the formation of these sensory organs remains poorly characterized as all related studies were performed in fixed tissue or *ex vivo*. To gain insight into the cell behavior that results in organ formation, we imaged the process directly on the mouth of an intact vertebrate – the optically transparent live zebrafish larva. We examined how early-differentiating *tg(fgf8a.dr17:gfp)* and type II *tg(Ola.plcβ2: egfp)* cells are displaced relative to type III *tg(tph1b:mCherry)* cells, and quantified the process using mean square displacement versus time interval [MSD(τ)] plots, which are widely used for cell and particle tracking (Bannai et al., 2007; Beltman et al., 2009; Cahalan and Parker, 2008; Grabher et al., 2007; Kusumi et al., 1993; Meijering et al., 2012; Monnier et al., 2012; Pézeron et al., 2008; Potel and Mackay, 1979; Ruthardt et al., 2011; Saxton and Jacobson, 1997; Sumen et al., 2004). We found that early-differentiating *tg(fgf8a.dr17:gfp)* and type II cells were displaced in random, directed or confined mode relative to type III cells that resulted in taste bud cell rearrangement, integration and maintenance. We particularly focused on the relative cell displacement that results in cell integration into the taste bud, and examined the role of 5-HT/ type III cells during this process.

RESULTS

tg(fgf8a.dr17) enhancer drives expression in early-differentiating taste bud cells

To follow taste bud development *in vivo*, we searched for regulatory elements that drive reporter expression at the early steps of organ formation and essentially retain it during taste bud cell differentiation. As zebrafish *fgf8a* is expressed in oropharyngeal epithelial (Kapsimali et al., 2011) and taste bud cells (Fig. S1J) and contributes to their formation (Kapsimali et al., 2011), we examined whether any of the known (Komisarczuk et al., 2009) *fgf8a* regulatory elements drives expression in taste buds. We found that prior to organ formation [55 hours post fertilization (hpf)], the enhancer *tg(fgf8a.dr17)* drives GFP expression in oropharyngeal epithelial cells (Fig. 1A-C).

To characterize the identity of *tg(fgf8a.dr17:gfp)* cells, epithelial and taste bud-related gene expression was analyzed using markers for type I, II and III cells, which were validated in fish (Kapsimali and Barlow, 2013; Kapsimali et al., 2011; Kirino et al., 2013; Matsumoto et al., 2013). Zebrafish *tg(fgf8a.dr17:gfp)*-expressing cells could co-express *sox2* (Fig. 1E; marker of oropharyngeal epithelial and taste bud cells), Prox1 (Fig. 1F; marker of early-differentiating taste bud cells), 5-HT (Fig. 1G; marker of Type-III cells, expressed from 59-60 hpf), Calb2 (Calretinin) and *plcb2* (Fig. 1D,H,I, arrowheads; markers of type II cells, expressed from 60-61 hpf and 65 hpf, respectively), *entpd2a* (Fig. 1J; marker of type I cells) or GABA (Fig. 1K; marker of mammalian type I and III cells, at 5 dpf; see also Fig. S1L,M). However, taste bud-related molecules were also expressed in cells without *tg(fgf8a.dr17:gfp)* expression; in particular, most *plcb2*- or Calb2-expressing cells were devoid of *tg(fgf8a.dr17:gfp)* expression (Fig. 1D,H,I, the number of cells per taste bud varies; for cell ratios, see Fig. S4H-N). One possibility is that *tg(fgf8a.dr17:gfp)* expression is dynamic; *tg(fgf8a.dr17:gfp)* is expressed early in taste bud differentiating cells but as their development proceeds, GFP expression is downregulated.

To examine whether *tg(fgf8a.dr17:gfp)* cells could differentiate into taste bud cells, we carried out fate-mapping by combining PsmOrange photoconversion and immunohistochemistry with
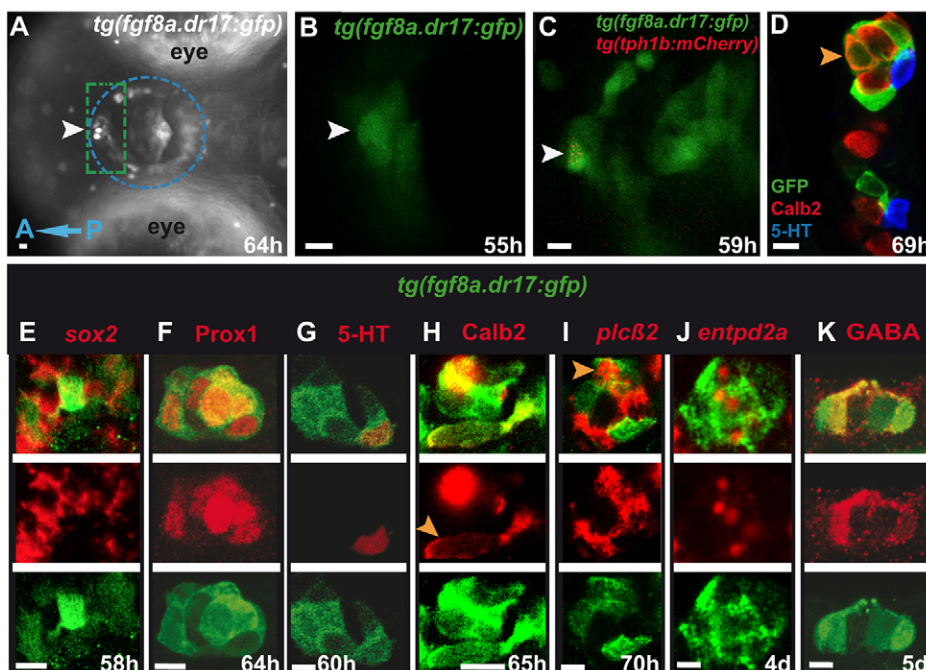

Fig. 1. *tg(fgf8a.dr17:gfp)* expression in developing taste bud cells. In all figures unless otherwise mentioned images are ventral views, anterior to the left. (A) Dissection scope. (B,C) 10 µm spinning-disk images, live larvae. In A, mouth epithelium (lips and wall) is within the blue dotted circle. Time-lapse imaging focused on anterior mouth epithelium (green dotted rectangle). White arrowheads indicate anterior-medial mouth where a taste bud forms (A,B) and a cell co-expressing *tg(fgf8a.dr17: gfp)* and *tg(tph1b:mCherry)* (C, red dots), respectively. (D-K) 2 µm confocal sections. In E-K, each column shows merge, taste bud marker (red) and *tg(fgf8a.dr17:gfp)* expression (green). In D,H,I, orange arrowheads indicate *tg(fgf8a.dr17:gfp)* cells that co-express Calb2 /*plcb2*. Scale bars: 10 µm.

available antibodies that recognize specific type II or III cell types in zebrafish (Kapsimali et al., 2011). Nuclear PSmOrange (Beretta et al., 2013) was mosaically expressed and photo-converted in *tg(fgf8a.dr17:gfp)*-expressing cells of the anterior mouth, prior to expression of 5-HT (type III) and Calb2 (type II) markers at 57 hpf (Fig. 2A-A‴,C-C‴). Five to eight hours later, immunohistochemistry revealed that cells co-expressing *tg(fgf8a. dr17:gfp)* and the photo-converted far-red emitting PSmOrange, could additionally express either 5-HT or Calb2 (*n*=24 embryos; *n*=5/11 cells expressing Calb2, *n*=5/13 cells expressing 5-HT; Fig. 2B-B‴,D-D‴). Therefore, *tg(fgf8a.dr17:gfp)*-expressing cells have the potential to differentiate into type II and type III cells.

tg(fgf8a.dr17:gfp)-expressing cells form taste buds

Given the early and wide *tg(fgf8a.dr17:gfp)* expression in oropharyngeal epithelium and taste bud cells, we used this transgenic line to follow *in vivo* taste bud formation. We focused on the easily accessible, anterior-mouth epithelium and performed time-lapse imaging analysis during time windows between 58 and 72 hpf. To distinguish between sites where taste buds form and the rest of the epithelium, *tg(fgf8a.dr17:gfp)* was combined with *tg(tph1b:mCherry)*, which is expressed in the earliest differentiating taste bud cell type in zebrafish – the 5-HT cell (Fig. 1C, Fig. S1A-C).

From 60 hpf onwards, *tg(fgf8a.dr17:gfp)* expression became intense in neighboring/adjacent cells that formed apparent groups, in the anterior mouth (Fig. 1A, Fig. 3A, Movie 1), later acquiring the taste bud pear-like shape (Fig. 4E-O, Movie 2). One of the grouped cells, initially expressing *tg(fgf8a.dr17:gfp)*, co-expressed *tg(tph1b: mCherry)* (Fig. 1C and Fig. 3A). During the 60 hpf to 5 dpf period, additional *tg(fgf8a.dr17:gfp)* cell groups were formed in between those formed early and organs of different cell size were spaced irregularly, 20-200 µm away from each other (Fig. S1K). Altogether the expression pattern, fate-mapping and time-lapse imaging analysis revealed that *tg(fgf8a.dr17:gfp)* expression is dynamic, becoming downregulated as cell differentiation advanced, allowing us to follow the early formation of a taste bud.

tg(fgf8a.dr17:gfp) cells are displaced in different modes during taste bud formation

Time-lapse imaging showed that *tg(fgf8a.dr17:gfp)* cells are displaced: rearranging at the site of a forming taste bud (Movie 1, green dot and Movie 2, yellow dot), moving from the epithelium towards a forming taste bud (Fig. 3A-H, Fig. 4D-I, Movies 1 and 2, blue dots) and between two neighboring developing organs (Fig. 4A-O,P-U, white arrowheads; Movie 2, blue dot; Movie 3, Table 1). Such diversity in taste bud cell displacement has not been described or characterized before. To start elucidating the mechanisms and significance of this diversity, here, we chose to focus on the assembly of the organ and analyzed displacement of *tg (fgf8a.dr17:gfp)* cells located at the site of the forming organ and those that joined a forming taste bud and were maintained within it. For this reason, we examined cell displacement relative to the taste bud where these cells assemble.

The 5-HT/type III cell was the first differentiated cell appearing in the *tg(fgf8a.dr17:gfp)* cell-forming organs (Fig. 1C and Fig. 3A) and was located the shortest distance from the mass center of the taste bud; we chose it as the reference cell (see Materials and Methods). The product of relative cell displacement [relative track of *tg(fgf8a. dr17:gfp)* cell to *tg(tph1b:mCherry)* cell] was informative about the behavior of one cell relative to the other, including small-scale displacements and it subtracted the drift of the anterior-dorsal dislocation of the mouth during larval growth. We analyzed time periods during which the cell of interest was grouped with (obvious contact with) or separate from the reference cell and the other cells in the taste bud where the reference cell was located.

To characterize cell displacement, MSD(τ) plots were made and classified by measuring their deviation from a purely diffusive regime. At first, we thus fitted the experimental results by a power law: MSD(τ)$\propto\tau^{\alpha}$ where τ corresponds to the time interval, as previously described (Kusumi et al., 1993; Meijering et al., 2012; Saxton and Jacobson, 1997; see Materials and Methods). In sum, α=1 and relative deviation (RD) $\simeq$1 correspond to pure diffusion (random motility) whereas α>1, RD>1 correspond to faster displacements and more exploratory behaviors than diffusion
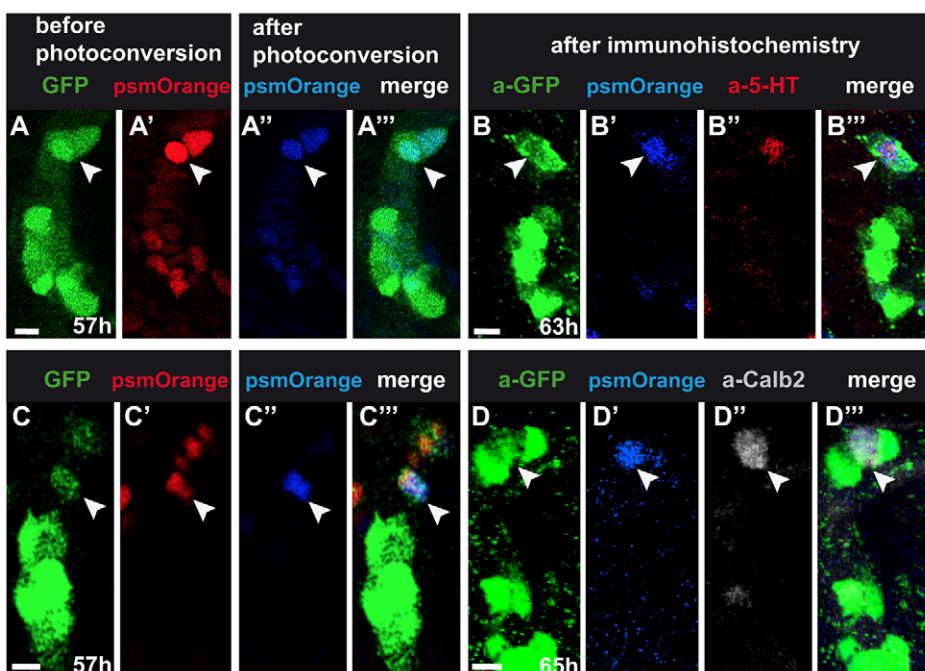

Fig. 2. Fate-mapping of *tg(fgf8a.dr17:gfp)* cells. 4 µm confocal projections of anterior mouth. One embryo per row, arrowheads indicate the same cell per row. (A,C) *tg(fgf8a. dr17:gfp)*, (A′,C′) non-photo-converted, (A″,C″) photo-converted nuclear PSmOrange expression in forming taste buds. (B,D) *tg(fgf8a.dr17:gfp)* expression detected with anti-GFP antibody. (B′,D′) Photo-converted nuclear PSmOrange after fixation. (B″,D″) Antibody-detected 5-HT or Calb2 expression. Scale bars: 10 µm.
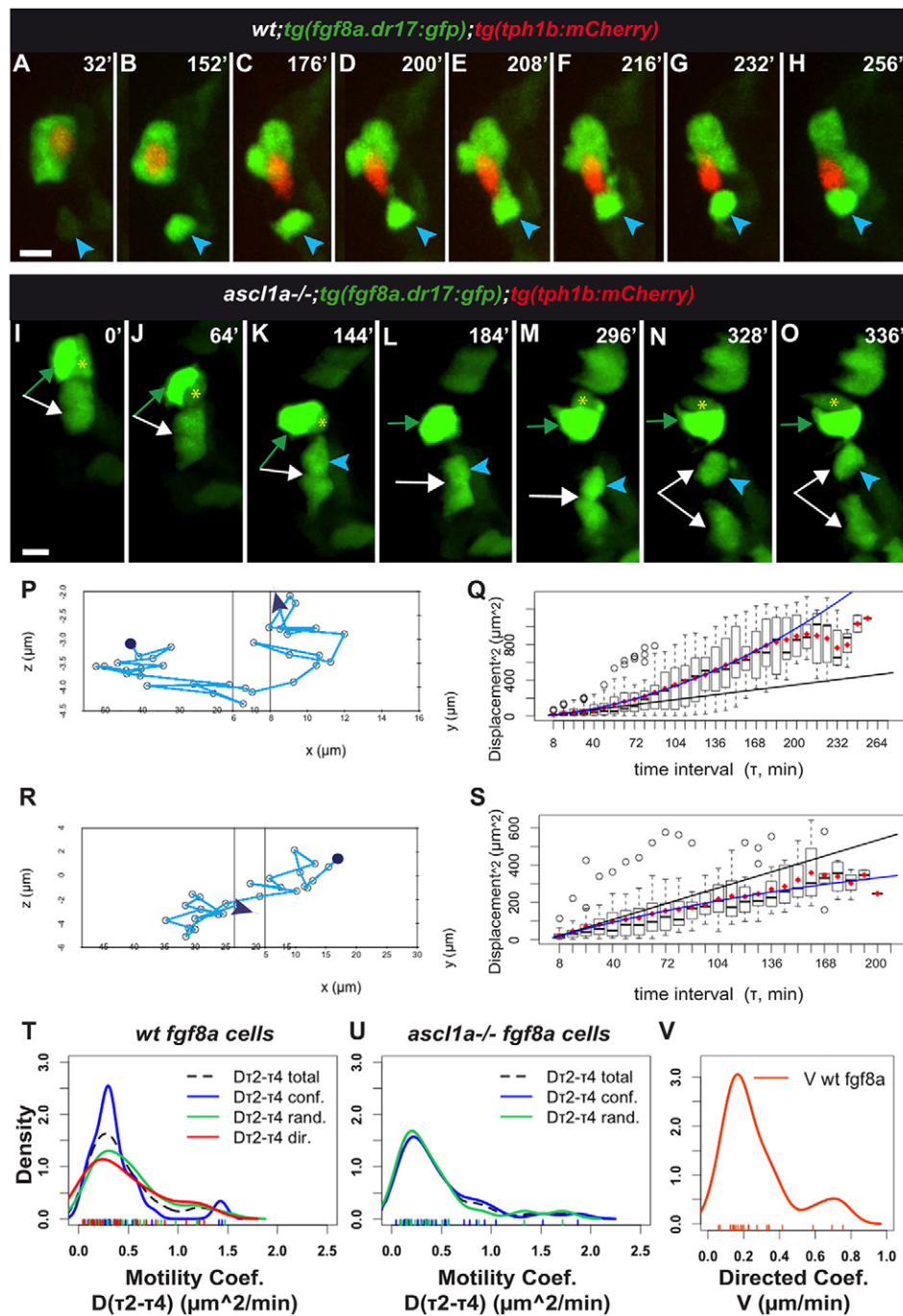
Fig. 3. *tg(fgf8a.dr17:gfp)* cell displacement during taste bud formation: differences between wild-type and *ascl1a⁻/⁻* larvae. In all figures with movie snapshots unless otherwise mentioned: spinning-disk z-stack image projections; time (minutes, top right) counts from time-lapse beginning. Anterior-medial mouth in live larvae. (A-H,I-O) Snapshots from Movies 1 and 7, respectively, started at approximately 60 hpf. (A-H) Wild-type. (I-O) *ascl1a⁻/⁻* mouth devoid of *tg(tph1b:mCherry)* expression. For detailed statistics, see Table 1, Fig. S2A-D, Tables S1,S2. Additional data in Appendix S1. *tg(fgf8a.dr17:gfp)* (green) cells form taste buds with (A-H) or without (I-O) *tg(tph1b:mCherry)* (red) expressing cells. In A-H, blue arrowhead indicates an epithelial *tg(fgf8a.dr17:gfp)* cell that joins the organ. In I-O, the arrows, arrowhead and asterisk indicate cells that initially formed an organ (green arrow- and yellow asterisk-marked cells overlap on z-axis in L). This organ splits over time and cells can remain together or become separate and regroup. (P,R) Tracks of relative displacement while individual cells (blue arrowheads in A-H, K-O, respectively) joined taste buds. Reference cell: in P, the *tg(tph1b:mCherry)* shown in A-H, time period 0-256min; in R, the *tg(fgf8a.dr17:gfp)* cell indicated by green arrow in I-O, time period 136-336 min. See additional data in Movie 1, blue dot; Movie 7, red dot; Appendix S1. (Q,S) MSD(τ) plots corresponding to tracks in P,R, respectively. Each boxplot shows all square displacement values for corresponding time intervals (each time interval 8 min, τ_1=one interval, τ_2=two intervals…); mean values shown by red diamonds. Black line is linear fit to τ_2-τ_4 mean values. Blue line is fit with the minimal summed-square of residuals; quadratic (Eqn. 6) in Q, showing directed motion; asymptotic (Eqn. 5) in S, tending towards a constant value *B*; confined displacement in a domain of size ~*B*. See Appendix S1. (T-V) Kernel (probability) density plots of coefficients for *tg(fgf8a.dr17:gfp)* cell motility. In T,U, motility coefficients $D\tau_2$-τ_4 come from similar continuous distributions in wild-type or *ascl1a⁻/⁻* larvae (see also Tables S1, S2, Fig. S2). In U,V, *ascl1a⁻/⁻;tg(fgf8a.dr17: gfp)* cells were devoid of directed motility [absence of *ascl1a⁻/⁻* $D\tau_2$-τ_4 and *V*, in U and V graphs, respectively]. Scale bars: 10 μm.

(directed motility) and α<1, RD<1 to slower and potentially, more confined trajectories.

During taste bud assembly, *tg(fgf8a.dr17:gfp)* cells, referenced to the closest taste bud/*tg(tph1b:mCherry)* cell, had linear, slower or faster than linear increase in the MSD, reminiscent of random, confined or directed motion, respectively (Table 1, Fig. 3P-Q, Appendix S1, Fig. S2A-D, Tables S1,S2). The motility coefficient *D* (increase of rate of explored surface) is determined using the first few points of the MSD curve. This fit is generally used because it determines *D* independent of the type of motion. In the case of taste bud *tg(fgf8a.dr17:gfp)* cells, the $D\tau_2$-τ_4 profiles (determined as in Kusumi et al., 1993) were not significantly different (Fig. 3T, Fig. S2A, Tables S1,S2). When the motion type

was taken into account, significant differences between the directed motility *D* distribution and that of other motility modes were found (Fig. S2B, Tables S1,S2). Altogether, these results showed that early forming taste bud cells had divergent modes of displacement relative to type III cells, revealing that taste bud formation is a more dynamic process than previously thought.

ascl1a activity in the 5-HT cell is required for directed motility and maintenance of *tg(fgf8a.dr17:gfp)* cells into the taste bud

We focused in particular on *tg(fgf8a.dr17:gfp)* cells that joined and were maintained within a taste bud. These cells had two characteristics: directed motility relative to the taste bud they
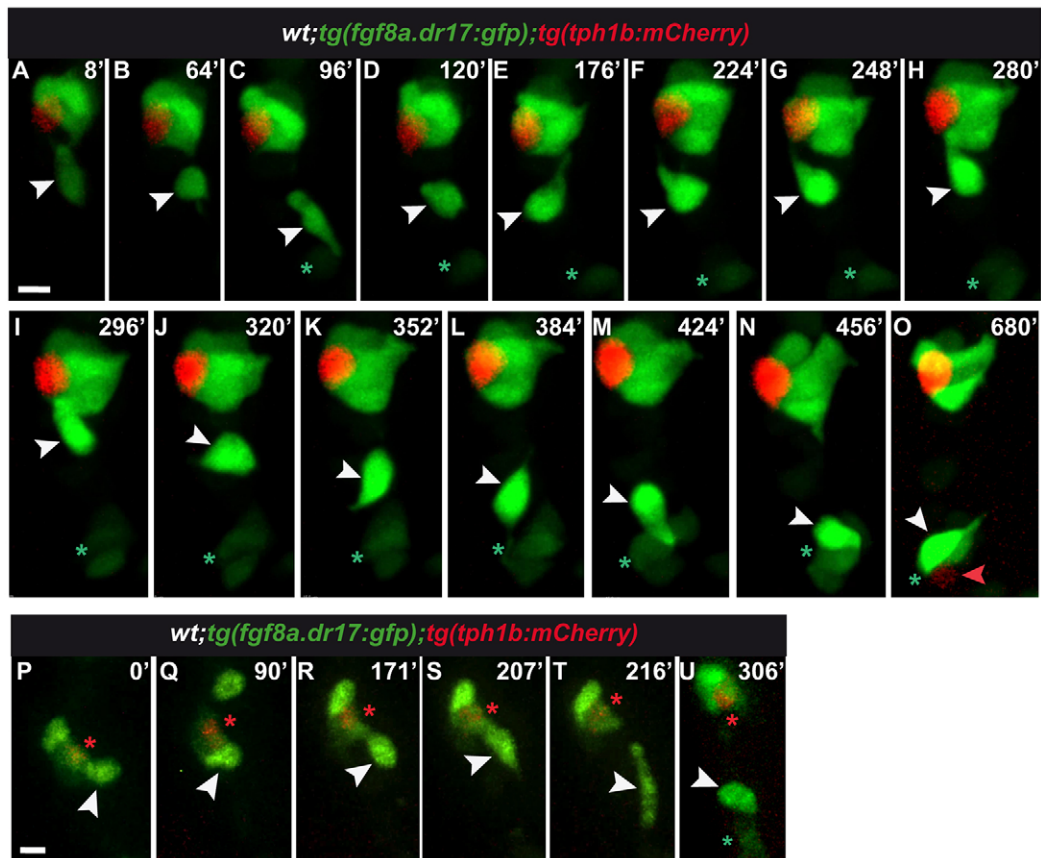
Fig. 4. Developing *tg(fgf8a.dr17:gfp)* cells can be displaced between neighboring forming taste buds. (A-O) Snapshots of Movie 2 with time-lapse started at approximately 65 hpf. Top of frame shows developing taste bud composed of *tg(fgf8a.dr17:gfp)* and *tg(tph1b:mCherry)* cells. In C-O, bottom of frame, the asterisk marks *tg(fgf8a.dr17:gfp)* cells forming a taste bud. White arrowheads indicate a single *tg(fgf8a.dr17:gfp)* cell displaced between the two taste buds (A-O); maintained in the upper taste bud (H,I) or joined to the bottom taste bud (M-O). Red arrowhead in O indicates a *tg(tph1b:mCherry)* cell, obvious after the integration of the displaced *tg(fgf8a.dr17:gfp)* cell (white arrowhead). Statistics are available in Table 1, Tables S1,S2, Fig. S2A-D, additional data in Appendix S1. (P-U) Snapshots of Movie 3 with time-lapse started at approximately 65 hpf. Red asterisk is next to a cell co-expressing *tg(fgf8a.dr17:gfp)* and *tg(tph1b:mCherry)*. White arrowhead indicates a *tg(fgf8a.dr17:gfp)* cell maintained within the taste bud for more than 180 min (P-S); it quits (T) towards another *tg(fgf8a.dr17:gfp)* expressing cell (U, green asterisk). Statistics are in Table 1, Tables S1,S2, Fig. S2A-D. Scale bars: 10 µm.

joined and contact with a *tg(tph1b:mCherry)* cell or a *tg(fgf8a.dr17: gfp)* cell that later expressed *tg(tph1b:mCherry)* when maintained by the taste bud (n=15, Table 1, Fig. 3A-H,P-Q, Fig. 4E-M, Fig. S2A-D, Tables S1,S2, Appendix S1, Movies 1 and 2). To examine whether type III cells could account for the dynamics of directed *tg(fgf8a.dr17:gfp)* cell motility and/or maintenance into the taste bud, our first approach was to focally ablate a *tg(tph1b:mCherry)* cell with a multi-photon laser and subsequently follow the development of the taste bud.

As a control, we analyzed the behavior of *tg(fgf8a.dr17:gfp)* cells after ablation of an adjacent *tg(fgf8a.dr17:gfp)* cell within the forming taste bud. In that case, taste bud *tg(fgf8a.dr17:gfp)* cells remained in or regained cell body contact with the *tg(tph1b: mCherry)* cell instead of quitting the ablation site (Fig. 5A-J, white arrowhead, Fig. 5A′-G′, gray and green dots; Movies 4 and 5). Additional *tg(fgf8a.dr17:gfp)* cells joined the group (Fig. 5A′-G′, blue arrowhead and dot; Movie 5) and all displacement modes relative to the *tg(tph1b:mCherry)* cell were observed (see statistics in Fig. S3). Therefore, *tg(fgf8a.dr17:gfp)* cells are dispensable for addition, directionality and maintenance of *tg(fgf8a.dr17:gfp)* cells during taste bud assembly.

By contrast, ablation of *tg(tph1b:mCherry)* cells resulted in disassembly of taste bud cells with two types of behavior: first, *tg(fgf8a.dr17:gfp)* cells left the ablated *tg(tph1b:mCherry)* cell site

and were displaced with relative directed motility towards neighboring taste buds (Fig. 5K-U, green and blue arrowheads; Movie 6, Fig. S3). The velocity V of these departing cells was increased compared with that of *tg(fgf8a.dr17:gfp)* cells that joined directionally the control, *tg(fgf8a.dr17:gfp)* cell-ablated site, described above (Fig. S3D). Second, *tg(fgf8a.dr17:gfp)* cells remained at the ablation site and displaced only in random or confined but not directed mode, relative to each other or neighboring epithelial *tg(fgf8a.dr17:gfp)* cells, to reform a cell group (Fig. 5K-U, pink dot; Fig. S3, Movie 6). Altogether, the cell ablation results showed that the *tg(tph1b:mCherry)* cell was required for directionality towards and contributed to maintenance of *tg(fgf8a. dr17:gfp)* cells into the taste bud to which it belonged, but it was dispensable for initial formation of a *tg(fgf8a.dr17:gfp)* cell group.

We hypothesized that directionality of *tg(fgf8a.dr17:gfp)* cells from the site of the ablated *tg(tph1b:mCherry)* cell towards another taste bud was due to the non-ablated *tg(tph1b:mCherry)* cells of neighboring taste buds. The second approach to examine whether the 5-HT/type III cell was required for *tg(fgf8a.dr17:gfp)* cell directionality, was to analyze taste bud cell behavior in *ascl1a*^{−/−} larvae, that are devoid of 5-HT/type III cells (Kapsimali et al., 2011; Fig. S4A-B,F,J).

The number of *tg(fgf8a.dr17:gfp)* cells was not significantly different between *ascl1a*^{−/−} and wild-type siblings (Fig. S4D-E,H,

Table 1. Summary of cell displacement profiles observed during taste bud development in wild-type and $ascl1a^{-/-}$ larvae

Behavior relative to taste bud*	Cells at site of forming taste bud	Cells joining forming taste bud	Data pooled for coefficient statistics	Data from:
wt *fgf8a*				6 embryos, 23 taste buds
Confined	34	0		
Random	20	8	Yes	
Directed	9‡		No	
From the epithelium		11	Yes	
Displaced from one taste bud to another		11 out of 19§	Yes	10 embryos, 42 taste buds
Total		22¶		
$ascl1a^{-/-}$ *fgf8a*				4 embryos, 17 taste buds
Confined	24		Yes	
Displaced from one taste bud to another		9	Yes	
Random	14		Yes	
Displaced from one taste bud to another**		7	Yes	
wt *plcb2*				4 embryos, 16 taste buds
Confined	14	0		
Random	2	11	Yes	
Directed	4‡‡	16		
$ascl1a^{-/-}$ *plcb2*				2 embryos, 10 taste buds
Confined	18			
Random	11			
Directed (all displaced from one taste bud to another)		8		

*Relative displacement of a cell towards/within the taste bud; the reference cell located in this taste bud. A single cell can change displacement behavior over time.
‡Relative directed motility for cells inside the taste bud was observed during the period of other cell incorporation (Appendix S1). These cells were not pooled with the ones that join the taste bud for coefficient statistics.
§Not a sufficient number of time points to determine motility for the other eight cells.
¶15 out of 22 had, in addition, directed motility during the first period of their maintenance within the taste bud (Appendix S1). However, there was no robust discriminating behavioral criterion to segment this time period from the rest of the cell maintenance time. Therefore, motility coefficients are not provided for this category. No data are available for the maintenance of 7 out of 22 cells.
**fgf8a* cells appeared in groups in *ascl1a^{-/-}$* larvae. Individual epithelial cells joining a taste bud as in the case of wild-type mouth were not obvious. Cells were displaced from one forming taste bud to another.
‡‡Directed motility during the first period of their maintenance within the taste bud. Motility coefficients are not provided for this category.

K-L). $ascl1a^{-/-};tg(fgf8a.dr17:gfp)$ cells appeared in groups in the developing mouth and cells were displaced from one forming taste bud towards another (Movie 7). Strikingly, analysis of MSD(τ) plots showed that $tg(fgf8a.dr17:gfp)$ cells in $ascl1a^{-/-}$ larvae were devoid of directed motility and had only random or confined displacement relative to the $tg(fgf8a.dr17:gfp)$ cell at the shortest distance from the mass center of the forming taste bud [as for the $tg(tph1b:mCherry)$ cell in the wild-type organ, organ to which they joined or they were maintained by; see Materials and Methods, Fig. 3I-O,R-V, Movies 7, 8, Appendix S1, Table 1, Tables S1,S2, Fig. S2A-D)]. These results oppose random displacement and favor cell migration as the mechanism for addition of $tg(fgf8a.dr17:gfp)$ differentiating cells into the taste bud.

If the directionality, provided by the $ascl1a$/5-HT synthetising cell, was linked to a broader, organizing activity of this cell that attracts $tg(fgf8a.dr17:gfp)$ cells to form an organ, one could expect that cells would be completely dispersed in $ascl1a^{-/-}$ oropharynx and organ formation entirely abolished. However, taste buds formed, in particular, in slightly increased numbers in $ascl1a^{-/-}$ compared with wild-type larvae (Fig. S4A-C; Kapsimali et al., 2011; Seta et al., 2011). How could organ formation be achieved in $ascl1a^{-/-}$ larvae? The time-lapse revealed that, in contrast to the wild type, not only individual $tg(fgf8a.dr17:gfp)$ cells, but also

small groups of 2-3 cells split from forming taste buds in $ascl1a^{-/-}$ larvae (Fig. 3I-M, Movie 7, blue, red, green dots; $n=5/12$ splitting groups, 3 $ascl1a^{-/-}$ embryos). Such a division of forming taste buds into smaller parts could account for the slight increase in the number of organs in $ascl1a^{-/-}$ larvae.

Altogether, the analysis of $tg(fgf8a.dr17:gfp)$ cell behavior in wild-type, taste bud cell ablated and $ascl1a^{-/-}$ larvae showed that early developing $tg(fgf8a.dr17:gfp)$ cells could form taste buds through relative random and confined displacement prior to $tg(tph1b:mCherry)$ cell differentiation (i.e. Fig. 4H-O, asterisk; Movie 2), additional $tg(fgf8a.dr17:gfp)$ cells could join the forming organ, and $ascl1a$ activity in the 5-HT cell was required for directed motility of $tg(fgf8a.dr17:gfp)$ cells towards and their maintenance within the taste bud.

Altered number and displacement behavior of type II cells contributes to taste bud formation in $ascl1a^{-/-}$ larvae

In addition to altered relative displacement of $tg(fgf8a.dr17:gfp)$ cells in $ascl1a^{-/-}$ mouth, taste buds had an increased number of Calb2/type II cells compared with the wild type (Kapsimali et al., 2011; Fig. S4G,I). Fate mapping showed that $tg(fgf8a.dr17:gfp)$ cells could differentiate into Calb2/type II cells, but expression patterns showed that these cells were mostly devoid of *tg(fgf8a.*
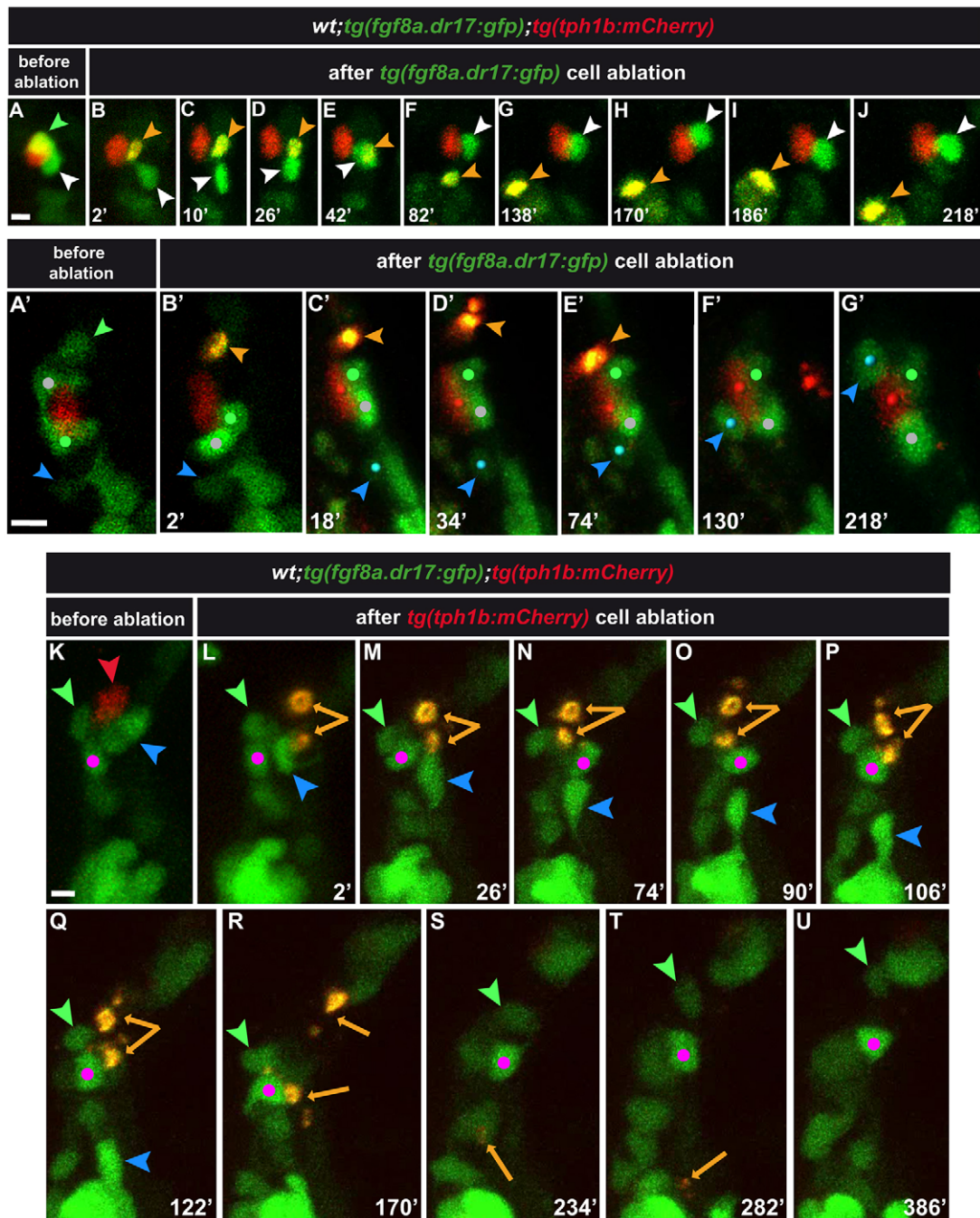
Fig. 5. Consequences of *tg(fgf8a.dr17:gfp)* or *tg(tph1b:mCherry)* cell ablation in taste bud formation. Anterior-lateral mouth, multi-photon *z*-stack image projections. The green (A,A′) and red (K) arrowheads indicate *tg(fgf8a.dr17:gfp)* and *tg(tph1b:mCherry)* cells that were ablated. (C-J,C′-G′,M-U) Snapshots of Movies 4-6, respectively. Time (min) after multi-photon laser ablation is shown. Statistics are in Fig. S3. Orange arrowheads (B-J,B′-E′) and arrows (L-T) indicate remaining fragments (yellow/orange) of ablated cells. In E, the remaining fragment overlaps with the neighboring *tg(fgf8a.dr17:gfp)* cell (*z*-projection). In A-J, white arrowhead indicates the *tg(fgf8a.dr17:gfp)* cell displaced away from (B-D) but re-established contact with (E-J) the *tg(tph1b:mCherry)* cell after ablation of the neighboring *tg(fgf8a.dr17:gfp)* cell. In A′-G′, white and green dots mark the position of intact *tg(fgf8a.dr17:gfp)* cells that maintained contact with the *tg(tph1b:mCherry)* cell after ablation of the neighboring *tg(fgf8a.dr17:gfp)* cell (orange arrowhead). Blue arrowhead/dot marks a *tg(fgf8a.dr17:gfp)* cell that joined the taste bud. In K-U, the three cells next to the *tg(tph1b:mCherry)*-ablated cell (orange arrows) are marked. Blue and green arrowheads mark cells that quitted the ablation site towards other taste buds. The pink dot marks a cell that remained in proximity to the ablation site and formed a group with *tg(fgf8a.dr17:gfp)* (low expression) cells that were not part of the targeted taste bud (see also Movie 6). Scale bars: 10 μm.

dr17:gfp) expression (Fig. 1D,H-I, Fig. 2C-D‴, Fig. S4L). These results prompted us to examine the relative displacement of type II cells in *ascl1a*^{−/−} larvae using the *tg(Ola.plcβ2:egfp)* line, which specifically expresses eGFP in differentiated type II cells (Fig. S1D-I; Aihara et al., 2007).

The first *tg(Ola.plcβ2:egfp)* cells were obvious in the wild-type mouth at 64 hpf, between *tg(tph1b:mCherry)* cells; they were displaced in relative random or directed motion to join them and they were maintained in confined mode adjacent to them (Fig. 6A-H, N-O, Fig. S2E-H, Tables S1,S2, Movie 9, Appendix S1, Table 1).
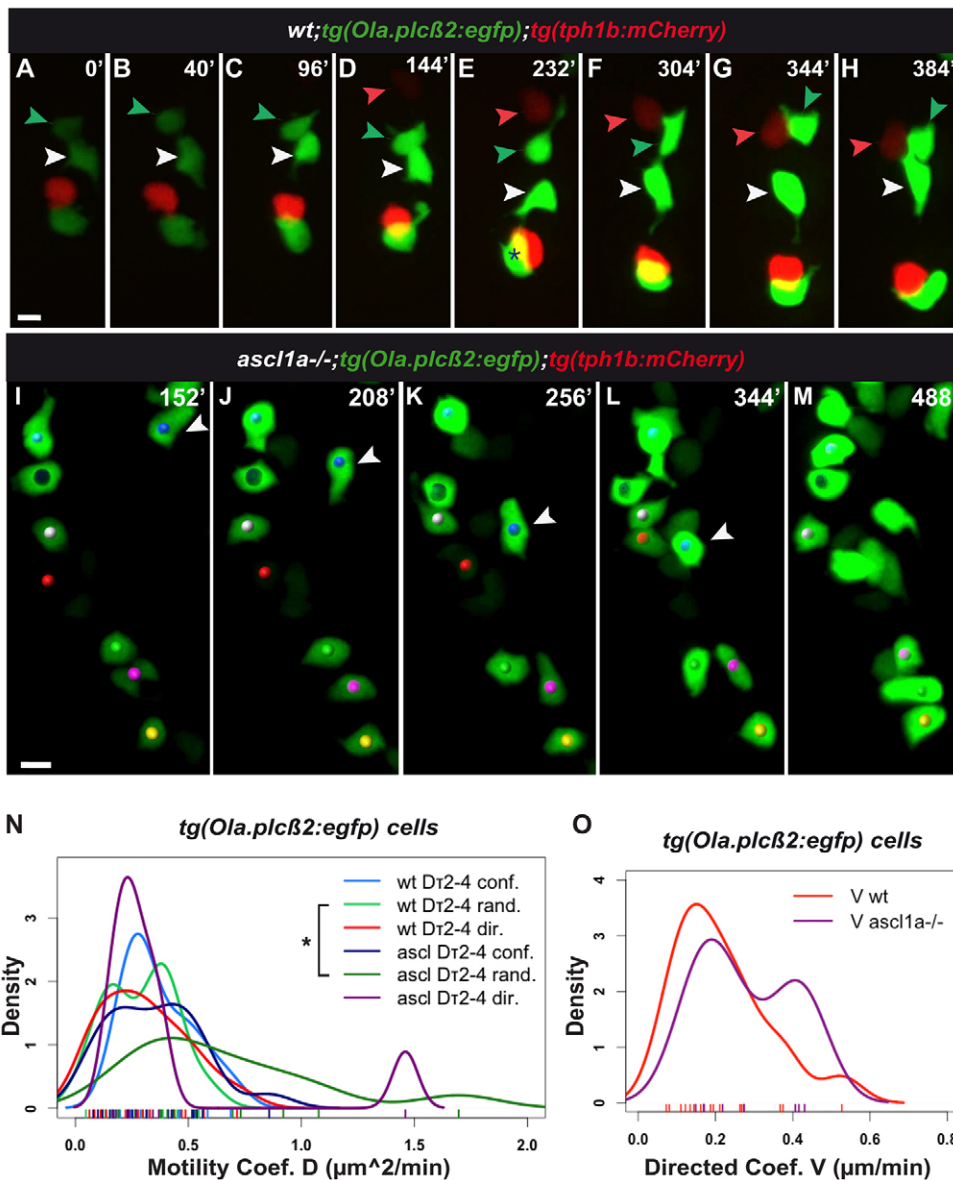
Fig. 6. tg(Ola.plcβ2:egfp) cells are displaced in three modes in the wild-type and ascl1a−/− mouth. (A-H,I-M) Snapshots of Movies 9 and 10, respectively. Both films started at approximately 64 hpf. Additional data is shown in Table 1, Tables S1,S2, Fig. S2E-H, Appendix S1. (A-H) tg(Ola.plcβ2:egfp) cells formed in proximity to tg(tph1b:mCherry) cells (red, red arrowhead), they were displaced among them (white, green arrowheads) and joined them. In E, asterisk shows overlap of two cells on z-axis. (I-M) ascl1a−/−;tg(Ola.plcβ2:egfp) cells form groups (yellow, pink, green dots at the bottom of the frame). White arrowhead indicates a cell that joined the cell indicated with a red dot in directed mode (Appendix S1). (N-O) Kernel plots of motility Dτ2-τ4 coefficients of tg(Ola.plcβ2:egfp) cells. In contrast to tg(fgf8a.dr17:gfp) cells, tg(Ola.plcβ2:egfp) cells show directed motility in ascl1a−/− mouth (compare with Fig. 3T-V). The significant difference between wild-type and ascl1a−/− relative random motility Dτ2-τ4 coefficients are highlighted with an asterisk (light and dark green; KS test, *P<0.05). Detailed statistics for all motility coefficients are provided in Tables S1,S2, Fig. S2. Scale bars: 10 µm.

However, in the mouth of ascl1a−/− larvae, tg(Ola.plcβ2:egfp) cells retained not only relative random and confined displacement, but also directed motion, in sharp contrast to tg(fgf8a.dr17:gfp) cells (Fig. 6I-O, Movie 10, Table 1, Appendix S1, Tables S1,S2, Fig. S2). Therefore, ascl1a activity is dispensable for the mode of relative displacement of type II cells.

In addition, comparison of the motility parameters of tg(Ola.plcβ2:egfp) cells between wild-type and ascl1a−/− larvae suggested different motility dynamics for this cell population (Fig. 6N, Fig. S2E-H). For instance, ascl1a activity could restrict the rate of relative random displacement of tg(Ola.plcβ2:egfp) cells (Fig. 6N, Fig. S2E-H; Tables S1,S2). In conclusion, the combination of altered number and dynamics of type II cells and the altered behavior of tg(fgf8a.dr17:gfp) cells (loss of directionality, cell group splitting) could account for taste bud formation in oral epithelium devoid of differentiated ascl1a/5-HT/type III cells.

DISCUSSION

In the present study, we used time-lapse imaging to directly observe taste bud formation in the zebrafish mouth. Three fluorescent-reporter transgenic lines were used to follow the behavior of different taste bud cell populations over time. tg(tph1b:mCherry) and tg(Ola.plcβ2:egfp) cells had specific expression in 5-HT/type III and type II cells, respectively. tg(fgf8a.dr17:gfp) had earlier and broader expression than the other two, in developing epithelial and taste bud cells with the potential to differentiate into type II and III cells and allowed us to follow the early steps of organ assembly. Using these tools, we obtained the first insight into the displacement mode of early and later forming taste bud cells and assessed the role of a specific cell type – the ascl1a/5-HT/type III cell – in taste bud assembly. We discuss the previously uncharacterized diversity of cell displacement modes during the formation of taste buds and propose a sequence of events that result in organ assembly under different circumstances, taking into account developmental timing and physiological constraints.

Analyzing cell displacement to understand taste bud formation

Cell lineage studies in mammals have extensively suggested that taste bud cells are derived from different progenitors, implying that

cell rearrangements occur within the epithelium to assemble a taste bud (e.g. Stone et al., 2002; also see Introduction). However, the nature of cell types (progenitors, differentiated), the modes of displacement (purely diffusive or not) and molecular signals contributing to cell displacement during taste bud formation remained unclear. Tracking of *tg(fgf8a.dr17:gfp)*, *tg(Ola.plcβ2: egfp)* and *tg(tph1b:mCherry)* cells within the zebrafish mouth epithelium revealed that several types of developing taste bud cells were displaced and in multiple ways, in a small volume of tissue: rearranging *in situ* to form an organ, from the epithelium into an organ and between organs. This led us to search for an efficient way to quantify diversity in cell displacement. We were inspired by particle, virus and immune cell displacement to use MSD(τ) plots (i.e. Beltman et al., 2009; Meijering et al., 2012; Ruthardt et al., 2011; Saxton and Jacobson, 1997). In contrast to other sensory organs, the taste bud structure is not stereotypical (Ohtubo and Yoshii, 2011; this study). As a starting point in addressing possible cell type interactions during taste bud assembly, we quantified relative cell trajectories to investigate the behavior of one taste bud cell to another over time periods during which cells were grouped (in contact) or separate.

MSD(τ) plots provided fine detail on the relative displacement of developing taste bud cells. Among the motility modes observed, confined trajectories (which correspond to MSD curves below pure diffusive movements) are the most complex to describe. Here, we classified as confined, all displacement plots in which MSD(τ) deviated negatively from random motility parameter values (RD<1, α<1). Confinement depends on coral geometry and number of obstacles (cells) that a cell encounters during displacement. Under certain circumstances, the centroid displacement could be minimal, implying immobility. Development of adequate tools to observe the entire epithelium, should allow more precise characterization of confinement and its functional significance for the taste bud.

Nevertheless, further analysis of the MSD(τ) plots (see Materials and Methods, Appendix S1, Tables S1,S2) revealed motility coefficients that provided information about relative cell displacement and resulted into two substantial novel findings. First, differentiating cell types could be displaced in distinct modes and this could be context dependent. Second, *ascl1a* activity in type III cells is required for directed motility of early-differentiating *tg(fgf8a.dr17:gfp)* cells and contributes to their maintenance within an organ.

How do differentiating cells assemble into a taste bud?

We propose that assembly of taste buds can be achieved in different ways. Within the early developing oral epithelium, adjacent/ neighboring *tg(fgf8a.dr17:gfp)* cells form organs through confined and/or random displacement. One of these cells has the potential to differentiate into a *ascl1a*/5-HT-synthesizing/type III cell. *ascl1a* activity is a prerequisite to direct additional *tg(fgf8a. dr17:gfp)* cells from the epithelium to the taste bud and contributes to their maintenance into the organ. This could be an efficient way to increase the number of cells, maintain them together and exclude organ formation in close proximity to those that already exist. In other words, *ascl1a* activity contributes to the initial steps of organ formation in several ways: establishment of 5-HT cell identity (Kapsimali et al., 2011; Seta et al., 2011), integration and maintenance of additional *tg(fgf8a.dr17:gfp)* cells and organ positioning/patterning within the epithelium (this study). There is a precedent for other transcription factors that control cell migration such as in the *Drosophila* optic lobe, where Ey/Pax6 is required for positioning of medulla neurons (Morante et al., 2011).

However, *ascl1a* is dispensable for relative directed motility of another taste bud cell population (type II) and taste buds can form in absence of differentiated *ascl1a*/5-HT/type III cells. This study is a first but not exhaustive analysis of type II cell displacement, showing that these cells can be displaced in a random, confined or directed manner and suggests that their motility dynamics are context dependent. The molecular signals underlying such diversity in type II motility remain to be elucidated.

In general, one could hypothesize that relative directed motility fulfils different tasks during organ development. For instance, in the case of type II cells, it might ensure adequate cell diversity within the organ (i.e. directionality between different type II subtypes, detecting bitter or umami etc.). Another argument in favor of correlation between displacement mode and function is that *tg(fgf8a.dr17:gfp)* cells and type II cells could be displaced between two organs (Movies 2, 3 and 9). Taste bud cell maintenance could be linked with correlated activity (Spitzer, 2006). Failure of a cell to correlate its activity within neighboring cells within an organ could lead to cell displacement towards a neighboring organ. Functional cell rearrangements have been observed within the lateral line sensory organs (Mirkovic et al., 2012). In this context, the role of innervation and/or support cells should also be considered in exploring the significance of cell displacement between taste buds.

Altogether, this study showed some flexibility in the mechanisms of organ assembly. In *ascl1a⁻/⁻* larvae, *tg(fgf8a.dr17:gfp)* cells retained random/confined displacement relative to each other, cell groups were partially split, the number of type II cells was increased and cell motility dynamics changed (i.e. Figs S2 and S4). Altogether, these modifications in cell behavior are likely to be sufficient to avoid dispersing taste bud cells throughout the epithelium. Taste bud cells are exposed to damaging chemicals, and multiple mechanisms to assemble and maintain cells could be an efficient strategy to ensure organ regeneration. By analyzing the formation of such a minute organ as the zebrafish taste bud, we show that diverse relative cell displacement is a mechanism that contributes to organ assembly and it will be worth examining whether this is widespread during organ/circuit formation in the nervous system.

MATERIALS AND METHODS
Fish strains
All procedures and protocols were in agreement with IBENS, French and European Union legislation for handling and maintaining zebrafish embryos and adults. Larvae were raised at 28-30°C. Embryos were obtained from natural spawning of wild-type (*AB×TL), *ascl1a(t25215/ t25215)* (Pogoda et al., 2006), *tg(fgf8a.dr17:gfp)* (Komisarczuk et al., 2009), *tg(Ola.plcβ2-1.6kb-EGFP)* (Aihara et al., 2007) [referred to as *tg (Ola.plcβ2:egfp)* here] and *tg(tph1b:mCherry)* (see below) zebrafish lines. *ascl1a⁻/⁻* larvae (59 hpf) were identified as previously described (Pogoda et al., 2006) and by the absence of oropharyngeal *tg(tph1b:mCherry)-* expressing cells. The phenotype of taste buds in *ascl1a* heterozygous (*ascl1a⁺/⁻*) larvae was indistinguishable from wild-type embryos (data not shown).

Construction of *tg(tph1b:mCherry)* zebrafish line
A previously identified (Kapsimali et al., 2011) 5 kb element immediately upstream of the *tph1b* gene was PCR amplified and cloned into an Tol2-mCherry expression vector containing the *cmlc2:egfp* transgenesis marker based on the *tol2* transposon (Tol2Kit) (Kwan et al., 2007). To generate transgenic fish, one-cell-stage embryos were injected with the *tol2-tph1b* promoter and transposase mRNA and screened for mCherry expression in taste buds. The taste bud expression profile of F1 *tg(tph1b:mCherry)* fish was confirmed by immunohistochemistry for 5-HT and mCherry (Fig. S1A-C).

In situ hybridization and immunohistochemistry

In situ hybridization and whole-mount immunohistochemistry were performed as previously described (Hauptmann and Gerster, 2000; Kapsimali et al., 2007). Zebrafish probes: *fgf8a* (Reifers et al., 1998), *sox2* (Cunliffe and Casaccia-Bonnefil, 2006), *plcb2* (Aihara et al., 2007), *entpd2a*: a 1024 bp fragment corresponding to 3′UTR sequence 2904-3927 bp of zebrafish *entpd2a.1* (NCBI NM_001004643.2) PCR amplified from genomic DNA extracted from 4 dpf embryos with primers: forward, 5′-GACACCGTAATAAAGCACGCTCTCAC-3′; reverse, 5′-CTGCACT-TTTGTAGCTGGCAACACTG-3′, subcloned into PCRII-Topo vector (Life Technologies) and verified by sequencing. The digoxigenin cRNA probe was synthesized after *Xho*I (Fermentas) digestion and SP6 (Roche) transcription. Primary antibodies were rabbit anti-GFP (1:1000, Torrey-Pines, TP401), rat anti-GFP (1:500, NacalaiTesque, 044084), mouse anti-mCherry (1:400, Clontech, 632543), rabbit anti-5HT (1:1000, Sigma, S5545), rabbit or mouse anti-Calb2 (1:1000, Swant, CR7699/3H and #6B3), mouse anti-Prox1 (1/500, Millipore, MAB5652), all validated in zebrafish (zfin.org). Secondary antibodies were conjugated to Alexa Fluor 350, 488, 568 or 647 (Invitrogen).

PSmOrange injection and photo-conversion

mRNA transcribed with mMessageMachine (Invitrogen) from a pcs2-H2B-PSmOrange construct (Beretta et al., 2013) was injected in 8-cell-stage *tg(fgf8a.dr17:gfp)* wild-type embryos incubated at 28.5-30°C in the dark and screened at 53 hpf for GFP and mosaic PSmOrange (orange/red) fluorescence in mouth epithelium. Selected larvae were mounted in 0.5% low-melting agarose, covered with embryo medium containing 0.017% Tricaine (Sigma) and 0.003% 1-phenyl-2 thiourea (Sigma). Image acquisition before and after photo-conversion was performed with 40× water-immersion objective (HCX Apo, NA=0.8) on a Leica SP5 confocal microscope. PSmOrange photo-conversion was performed with 1 mW power of Argon 488 nm laser (30-40 scans at 200 Hz, 0.5 s/frame, 5× zoom, compromising between laser power and photo-bleaching). Photo-converted embryos were left to grow for 5-8 h in the dark and processed for immunohistochemistry. As antibodies specific to photo-converted PSmOrange are unavailable, precautions were taken to keep intact the photo-converted PSmOrange [working in the dark, short 30-45 min fixation in 4% paraformaldehyde in phosphate saline buffer (PBS), three intermediate 5 min washes with 0.1% Triton X-100 in PBS, antibody incubation in 1% BSA, 1% DMSO, 0.5% Triton X-100 in PBS at 4°C for 10 h]. Primary and secondary antibodies were as described above.

Image acquisition on fixed tissue

Fluorescent images were acquired with a Leica SP5 confocal microscope using 25×(PL Fluotar)/40×(HCX PL APO CS) oil immersion objectives. A series of images was acquired at 0.5-1 μm intervals. ImageJ (NIH), Adobe Photoshop and Illustrator were used to analyze stacks, adjust brightness/contrast and mount images. Three-dimensional reconstructions and cell counting were carried out using Imaris (BitPlane).

Embryo mounting for time-lapse live imaging

Larvae were immobilized using Tricaine and mounted in plasma-thrombin medium (Renaud et al., 2011) with the mouth towards the microscope objective on a coverslip of glass-covered Petri dish (Mattek).

Spinning-disk imaging in live larvae

Time-lapse imaging was performed on zebrafish larvae in time windows between 58 and 72 hpf. Occasionally, stacks were acquired between 3 and 5 dpf. Taste bud cells were imaged on a spinning disk (CSU-X1, Yokogawa Electric Corporation) confocal microscope using 40× water-immersion objective lens (Apochromat LWD NA 1.15) on a TiE Eclipse (Nikon) microscope, equipped with Perfect Focus System (Nikon) and heating enclosure. Illumination was provided by 491 nm and 561 nm lasers (Roper Scientifics); 525-545 nm and 605-664 nm filters (Semrock) were used for GFP and mCherry detection. Image stacks were acquired using EMCCD (Evolve, Photometrics) camera every 8 (or 9) min, at 0.6-1 μm z-step and 500 ms image intervals using approximately 100 ms exposure

time. Microscope system automation was controlled with Metamorph software (Molecular Devices).

Multi-photon laser cell ablations

Cell ablations were performed with a custom-built random-access two-photon laser-scanning microscope (Otsu et al., 2008), where both *x* and *y* scanning are operated by acousto-optic deflectors (AODs). These custom-built non-mechanical beam-steering devices (A-A Opto-Electronic) can redirect the laser beam in 10 μs. To operate AODs and run scanning procedures, a custom-made user interface was programmed in LabView (National Instruments). The AOD acoustic frequency drive was generated combining a Direct Digital Synthesizer and a fast (10 ns) power amplifier (A-A Opto-Electronics). Two-photon excitation was produced by infrared Ti-Sa pulsed chameleon vision laser (Coherent) tuned to 825 nm coupled to the microscope (Slicescope, Scientifica). The microscope was equipped with a 25× objective LUMPlanFL/IR/NA-0.95, Leica microsystems). Fluorescence photons were detected by cooled AsGaP H10769PA-40 photomultipliers (Hamamatsu) in transfluorescence and epifluorescence pathways, using 641-75 nm and 510-584 nm bandpass filters (Semrock) for both pathways. Ablation was produced in a confined optical resolution spot (*x-y*: 300 nm, *z*: 1 μm) with 500 mw ±10% laser power and 200 μs dwell time. Under these conditions, only one cell was ablated and neighboring cells were not affected. Subsequently, stacks of images were obtained with 3-4 μs dwell time scanning and 20 mW laser power.

Statistical analysis

This was performed using the freely available software R (http://www.r-project.org). For each parameter, normal distribution was assessed with Shapiro–Wilk test and rejected if $P<0.05$. Welch *t*-test was used to compare parameters with normal distribution. Otherwise, the non-parametric two-sample Kolmogorov–Smirnov test was applied.

Cell tracking and analysis of cell displacement modes
Segmentation

Spinning-disk and multi-photon *z*-stacks acquired over time were visualized and processed for cell segmentation with ImarisTrack (BitPlane). Segmentation was then manually verified for each cell at each time point and found to be optimal in wild-type cell groups containing up to three *tg(fgf8a.dr17:gfp)* or *tg(Ola.plcβ2-1.6kb-EGFP)* cells and for isolated cells moving in the epithelium and from/to taste buds. The *ascl1a⁻/⁻ ; tg(fgf8a.dr17:gfp)* cells could be more tightly packed during early taste bud development; to optimize *tg(fgf8a.dr17:gfp)* cell segmentation in that case, *ascl1a⁻/⁻* (and wild-type siblings) with ubiquitous expression of membrane mCherry (by mRNA injection at 1-cell stage) were additionally analyzed. Owing to anterior-dorsal movement of the mouth at these developmental stages, to adequately follow taste bud development, 100-130 μm *z*-stacks were acquired over time, and for clarity, the membrane mCherry was omitted in the projection images and movies.

Defining time periods for MSD(τ) analysis

A single cell could change behavior when located within the epithelium or a forming taste bud, joining or quitting an organ. The criterion for defining time periods was whether cells of interest were in obvious contact with or separated from cells in the reference taste bud (the organ that cells of interest joined or were maintained).

Reference cells

Coordinates (*x*,*y*,*z*) of the center of mass of each cell were obtained by Imaris for each time point. To calculate cell displacement, we used reference cells ('refcell') in the taste bud where the cells assembled (joined/maintained). This also allowed subtraction of the drift due to mouth growth and anterior-dorsal shift (Fig. S1L). In wild-type larvae, the *tg(tph1b:mCherry)* cell is at the shortest distance from the mass center of the forming taste bud, (*n*=12/12 taste buds, data not shown); therefore, *tg(fgf8a.dr17:egfp)* or *tg(Ola.plcβ2:egfp)* cell displacement was calculated relative to the *tg(tph1b:mCherry)* cell. In the absence of *tg(tph1b:mCherry)* in wild-type or *ascl1a⁻/⁻* larvae, the reference

was the *tg(fgf8a.dr17:gfp)* or *tg(Ola.plcβ2:egfp)* cell found at the shortest distance from the mass center of the forming organs. The same rules applied in cell ablation experiments. In cases where *ascl1a$^{-/-}$;tg(Ola.plcβ2:egfp)* cells were not tightly packed, displacement was additionally calculated relative to a second cell of the group and/or that they mostly contacted during the movie; results regarding the displacement mode were found consistent among these plots.

Quantification of displacement

If *r* is the cell position at time point *i*, the mean squared displacement (MSD) for *N* positions and time intervals τ is computed as:

$$\mathrm{MSD}(\tau) = \frac{1}{N-\tau}\sum_{i=1}^{N-\tau}|r_{i+\tau}-r_i|^2, \tag{1}$$

but in this case,

$$|r_{i+\tau}-r_i|^2 \tag{2}$$

was replaced by:

$$\begin{aligned}\{\ &[(x(\mathrm{cell})_{i+\tau}-x(\mathrm{refcell})_{i+\tau})-(x(\mathrm{cell})_i-x(\mathrm{refcell})_i)]^2+\\ &[(y(\mathrm{cell})_{i+\tau}-y(\mathrm{refcell})_{i+\tau})-(y(\mathrm{cell})_i-y(\mathrm{refcell})_i)]^2+\\ &[(z(\mathrm{cell})_{i+\tau}-z(\mathrm{refcell})_{i+\tau})-(z(\mathrm{cell})_i-z(\mathrm{refcell})_i)]^2\ \}\ ,\end{aligned} \tag{3}$$

to take into account the cell position relative to the reference cell (refcell).

Depending on the type of motility, MSD is described in three dimensions by the equations (Meijering et al., 2012; Monnier et al., 2012):

$$\mathrm{MSD}(\tau) = 6D\tau, \tag{4}$$

$$\mathrm{MSD}(\tau) = B^2(1 - e^{-\frac{6D\tau}{B^2}}), \tag{5}$$

$$\mathrm{MSD}(\tau) = 6D\tau + V^2\tau^2, \tag{6}$$

for random, confined or directed motion, respectively. *D* is the motility (diffusion) coefficient (μm^2/min), *B*, confinement radius (μm) and *V*, mean velocity (μm/min) (Kusumi et al., 1993; Meijering et al., 2012; Monnier et al., 2012; Saxton and Jacobson, 1997).

Classification of MSD(τ) plots

To estimate deviation of the MSD plot from linear fit (random motility), we plotted a linear fit (black line in the plots) on the MSD values at τ$_2$,τ$_3$,τ$_4$ (Kusumi et al., 1993). The motility coefficient *D*τ$_2$-τ$_4$ is not significantly affected by non-random motion. If the distribution of relative deviation [RD, ratio of observed MSD to MSD extrapolated from the (τ$_2$-τ$_4$) fit, at given interval] peaks at 1, motility is random; RD>1, directed; RD<1, confined (Appendix S1).

In parallel, we plotted log(MSD) to log(τ) for (τ>τ$_4$) and determined the exponent α (see equation for anomalous diffusion, reviewed by Saxton and Jacobson, 1997):

$$\mathrm{MSD}(\tau) = D_\alpha\tau^\alpha. \tag{7}$$

α=1 signifies random; α>1, directed (threshold here, α≥1.1) and α<1, constrained/confined (here, threshold α<0.9).

To characterize the MSD(τ) curve, plots were checked in priority for linear fit (Eqn. 4). Residuals were plotted against fitted values to assess constant variance (i.e. to check that residuals did not follow any regular pattern). Residual normality was assessed using quantile (residuals against normal distribution, checked for absence of skewing or humps) and density plots. If residual constant variance and normality were respected, a non-constant variance score test (chi-square) was also applied and *r*-squared calculated. If residual variance was not constant when applying a linear fit, or the RD and α values suggested clearly another fit, we checked for asymptotic or quadratic dependence of the MSD(τ) plot (Eqns 5 and 6). The fit was again checked for constant variance and normal distribution of residuals to be validated. In some cases, outliers were identified and excluded [i.e. residual plots, Grubbs

and Dixons tests, in R (http://www.r-project.org)]. The fit with minimal summed-square of residuals was selected and (r^2=1−SS$_{\mathrm{res}}$/SS$_{\mathrm{tot}}$) was calculated (SS$_{\mathrm{res}}$ is the sum of square of the residuals (the value minimized by the nonlinear regression) and SS$_{\mathrm{tot}}$=sum{[y−mean(y)]^2} (the sum of the squared differences between the data points and the average of the data points). The closest the r^2 to 1 the better the fit (Motulsky and Ransnas, 1987). In all cases, we found good agreement among RD, α and curve fit about the displacement type. Examples of MSD(τ) plots, are provided in Appendix S1. R scripts are available upon request.

Competing interests
The authors declare no competing or financial interests.

Author contributions
M.K. conceived the project, M.S., A.-L.K., B.M., R.L., A.Z.K., N.T., A.L., S.O., M.K. performed experiments, M.S., A.-L.K., S.A.R., A.J., B.M., M.K. performed data analysis, M.K., S.O., S.A.R., K.A., T.S.B., prepared and edited the manuscript.

Supplementary information
Supplementary information available online at
http://dev.biologists.org/lookup/suppl/doi:10.1242/dev.134817/-/DC1

References
Aihara, Y., Yasuoka, A., Yoshida, Y., Ohmoto, M., Shimizu-Ibuka, A., Misaka, T., Furutani-Seiki, M., Matsumoto, I. and Abe, K. (2007). Transgenic labeling of taste receptor cells in model fish under the control of the 5′-upstream region of medaka phospholipase C-beta 2 gene. *Gene Expr. Patterns* **7**, 149-157.

Aihara, E., Mahe, M. M., Schumacher, M. A., Matthis, A. L., Feng, R., Ren, W., Noah, T. K., Matsu-Ura, T., Moore, S. R., Hong, C. I. et al. (2015). Characterization of stem/progenitor cell cycle using murine circumvallate papilla taste bud organoid. *Sci. Rep.* **5**, 17185.

Bannai, H., Lévi, S., Schweizer, C., Dahan, M. and Triller, A. (2007). Imaging the lateral diffusion of membrane molecules with quantum dots. *Nat. Protoc.* **1**, 2628-2634.

Barlow, L. A. and Klein, O. D. (2015). Developing and regenerating a sense of taste. *Curr. Top. Dev. Biol.* **111**, 401-419.

Barlow, L. and Northcutt, R. G. (1995). Embryonic origin of amphibian taste buds. *Dev. Biol.* **169**, 273-285.

Barlow, L. A. and Northcutt, R. G. (1997). Taste buds develop autonomously from endoderm without induction by cephalic neural crest or paraxial mesoderm. *Development* **124**, 949-957.

Barretto, R. P. J., Gillis-Smith, S., Chandrashekar, J., Yarmolinsky, D. A., Schnitzer, M. J., Ryba, N. J. P. and Zuker, C. S. (2015). The neural representation of taste quality at the periphery. *Nature* **517**, 373-376.

Beites, C. L., Hollenbeck, P. L. W., Kim, J., Lovell-Badge, R., Lander, A. D. and Calof, A. L. (2009). Follistatin modulates a BMP autoregulatory loop to control the size and patterning of sensory domains in the developing tongue. *Development* **136**, 2187-2197.

Beltman, J. B., Marée, A. F. M. and de Boer, R. J. (2009). Analysing immune cell migration. *Nat. Rev. Immunol.* **9**, 789-798.

Beretta, C. A., Dross, N., Bankhead, P. and Carl, M. (2013). The ventral habenulae of zebrafish develop in prosomere 2 dependent on Tcf7l2 function. *Neural Dev.* **8**, 19.

Cahalan, M. D. and Parker, I. (2008). Choreography of cell motility and interaction dynamics imaged by two-photon microscopy in lymphoid organs. *Annu. Rev. Immunol.* **26**, 585-626.

DEVELOPMENT

Chandrashekar, J., Hoon, M. A., Ryba, N. J. P. and Zuker, C. S. (2006). The receptors and cells for mammalian taste. *Nature* **444**, 288-294.

Chandrashekar, J., Yarmolinsky, D., von Buchholtz, L., Oka, Y., Sly, W., Ryba, N. J. P. and Zuker, C. S. (2009). The taste of carbonation. *Science* **326**, 443-445.

Chaudhari, N. and Roper, S. D. (2010). The cell biology of taste. *J. Cell Biol.* **190**, 285-296.

Cunliffe, V. T. and Casaccia-Bonnefil, P. (2006). Histone deacetylase 1 is essential for oligodendrocyte specification in the zebrafish CNS. *Mech. Dev.* **123**, 24-30.

Dvoryanchikov, G., Huang, Y. A., Barro-Soria, R., Chaudhari, N. and Roper, S. D. (2011). GABA, its receptors, and GABAergic inhibition in mouse taste buds. *J. Neurosci.* **31**, 5782-5791.

Finger, T. E., Danilova, V., Barrows, J., Bartel, D. L., Vigers, A. J., Stone, L., Hellekant, G. and Kinnamon, S. C. (2005). ATP signaling is crucial for communication from taste buds to gustatory nerves. *Science* **310**, 1495-1499.

Gaillard, D., Xu, M., Liu, F., Millar, S. E. and Barlow, L. A. (2015). β-catenin signaling biases multipotent lingual epithelial progenitors to differentiate and acquire specific taste cell fates. *PLoS Genet.* **11**, e1005208.

Grabher, C., Cliffe, A., Miura, K., Hayflick, J., Pepperkok, R., Rørth, P. and Wittbrodt, J. (2007). Birth and life of tissue macrophages and their migration in embryogenesis and inflammation in medaka. *J. Leukoc. Biol.* **81**, 263-271.

Hauptmann, G. and Gerster, T. (2000). Multicolor whole-mount in situ hybridization. *Methods Mol. Biol.* **137**, 139-148.

Huang, Y. A., Dando, R. and Roper, S. D. (2009). Autocrine and paracrine roles for ATP and serotonin in mouse taste buds. *J. Neurosci.* **29**, 13909-13918.

Huang, Y. A., Pereira, E. and Roper, S. D. (2011a). Acid stimulation (sour taste) elicits GABA and serotonin release from mouse taste cells. *PLoS ONE* **6**, e25471.

Huang, Y. A., Stone, L. M., Pereira, E., Yang, R., Kinnamon, J. C., Dvoryanchikov, G., Chaudhari, N., Finger, T. E., Kinnamon, S. C. and Roper, S. D. (2011b). Knocking out P2X receptors reduces transmitter secretion in taste buds. *J. Neurosci.* **31**, 13654-13661.

Iwatsuki, K., Liu, H.-X., Grónder, A., Singer, M. A., Lane, T. F., Grosschedl, R., Mistretta, C. M. and Margolskee, R. F. (2007). Wnt signaling interacts with Shh to regulate taste papilla development. *Proc. Natl. Acad. Sci. USA* **104**, 2253-2258.

Kapsimali, M. and Barlow, L. A. (2013). Developing a sense of taste. *Semin. Cell Dev. Biol.* **24**, 200-209.

Kapsimali, M., Kloosterman, W. P., de Bruijn, E., Rosa, F., Plasterk, R. H. A. and Wilson, S. W. (2007). MicroRNAs show a wide diversity of expression profiles in the developing and mature central nervous system. *Genome Biol.* **8**, R173.

Kapsimali, M., Kaushik, A.-L., Gibon, G., Dirian, L., Ernest, S. and Rosa, F. M. (2011). Fgf signaling controls pharyngeal taste bud formation through miR-200 and Delta-Notch activity. *Development* **138**, 3473-3484.

Kinnamon, S. C. and Finger, T. E. (2013). A taste for ATP: neurotransmission in taste buds. *Front. Cell Neurosci.* **7**, 264.

Kirino, M., Parnes, J., Hansen, A., Kiyohara, S. and Finger, T. E. (2013). Evolutionary origins of taste buds: phylogenetic analysis of purinergic neurotransmission in epithelial chemosensors. *Open Biol.* **3**, 130015.

Kist, R., Watson, M., Crosier, M., Robinson, M., Fuchs, J., Reichelt, J. and Peters, H. (2014). The formation of endoderm-derived taste sensory organs requires a Pax9-dependent expansion of embryonic taste bud progenitor cells. *PLoS Genet.* **10**, e1004709.

Komisarczuk, A. Z., Kawakami, K. and Becker, T. S. (2009). Cis-regulation and chromosomal rearrangement of the fgf8 locus after the teleost/tetrapod split. *Dev. Biol.* **336**, 301-312.

Kusumi, A., Sako, Y. and Yamamoto, M. (1993). Confined lateral diffusion of membrane receptors as studied by single particle tracking (nanovid microscopy). Effects of calcium-induced differentiation in cultured epithelial cells. *Biophys. J.* **65**, 2021-2040.

Kwan, K. M., Fujimoto, E., Grabher, C., Mangum, B. D., Hardy, M. E., Campbell, D. S., Parant, J. M., Yost, H. J., Kanki, J. P. and Chien, C.-B. (2007). The Tol2kit: a multisite gateway-based construction kit for Tol2 transposon transgenesis constructs. *Dev. Dyn.* **236**, 3088-3099.

Liu, F., Thirumangalathu, S., Gallant, N. M., Yang, S. H., Stoick-Cooper, C. L., Reddy, S. T., Andl, T., Taketo, M. M., Dlugosz, A. A., Moon, R. T. et al. (2007). Wnt-beta-catenin signaling initiates taste papilla development. *Nat. Genet.* **39**, 106-112.

Liu, H.-X., Komatsu, Y., Mishina, Y. and Mistretta, C. M. (2012). Neural crest contribution to lingual mesenchyme, epithelium and developing taste papillae and taste buds. *Dev. Biol.* **368**, 294-303.

Liu, H. X., Ermilov, A., Grachtchouk, M., Li, L., Gumucio, D. L., Dlugosz, A. A. and Mistretta, C. M. (2013). Multiple Shh signaling centers participate in fungiform papilla and taste bud formation and maintenance. *Dev. Biol.* **382**, 82-97.

Matsumoto, I., Ohmoto, M., Narukawa, M., Yoshihara, Y. and Abe, K. (2011). Skn-1a (Pou2f3) specifies taste receptor cell lineage. *Nat. Neurosci.* **14**, 685-687.

Matsumoto, I., Ohmoto, M. and Abe, K. (2013). Functional diversification of taste cells in vertebrates. *Semin. Cell Dev. Biol.* **24**, 210-214.

Meijering, E., Dzyubachyk, O. and Smal, I. (2012). Methods for cell and particle tracking. *Methods Enzymol.* **504**, 183-200.

Mirkovic, I., Pylawka, S. and Hudspeth, A. J. (2012). Rearrangements between differentiating hair cells coordinate planar polarity and the establishment of mirror symmetry in lateral-line neuromasts. *Biol. Open* **1**, 498-505.

Mistretta, C. M., Liu, H.-X., Gaffield, W. and MacCallum, D. K. (2003). Cyclopamine and jervine in embryonic rat tongue cultures demonstrate a role for Shh signaling in taste papilla development and patterning: fungiform papillae double in number and form in novel locations in dorsal lingual epithelium. *Dev. Biol.* **254**, 1-18.

Miura, H., Scott, J. K., Harada, S. and Barlow, L. A. (2014). Sonic hedgehog-expressing basal cells are general post-mitotic precursors of functional taste receptor cells. *Dev. Dyn.* **243**, 1286-1297.

Monnier, N., Guo, S.-M., Mori, M., He, J., Lénárt, P. and Bathe, M. (2012). Bayesian approach to MSD-based analysis of particle motion in live cells. *Biophys. J.* **103**, 616-626.

Morante, J., Erclik, T. and Desplan, C. (2011). Cell migration in Drosophila optic lobe neurons is controlled by eyeless/Pax6. *Development* **138**, 687-693.

Motulsky, H. J. and Ransnas, L. A. (1987). Fitting curves to data using nonlinear regression: a practical and nonmathematical review. *FASEB J.* **1**, 365-374.

Nguyen, H. M., Reyland, M. E. and Barlow, L. A. (2012). Mechanisms of taste bud cell loss after head and neck irradiation. *J. Neurosci.* **32**, 3474-3484.

Ohtubo, Y. and Yoshii, K. (2011). Quantitative analysis of taste bud cell numbers in fungiform and soft palate taste buds of mice. *Brain Res.* **1367**, 13-21.

Okubo, T., Clark, C. and Hogan, B. L. M. (2009). Cell lineage mapping of taste bud cells and keratinocytes in the mouse tongue and soft palate. *Stem Cells* **27**, 442-450.

Ota, M. S., Kaneko, Y., Kondo, K., Ogishima, S., Tanaka, H., Eto, K. and Kondo, T. (2009). Combined in silico and in vivo analyses reveal role of Hes1 in taste cell differentiation. *PLoS Genet.* **5**, e1000443.

Otsu, Y., Bormuth, V., Wong, J., Mathieu, B., Dugué, G. P., Feltz, A. and Dieudonné, S. (2008). Optical monitoring of neuronal activity at high frame rate with a digital random-access multiphoton (RAMP) microscope. *J. Neurosci. Methods* **173**, 259-270.

Perea-Martinez, I., Nagai, T. and Chaudhari, N. (2013). Functional cell types in taste buds have distinct longevities. *PLoS ONE* **8**, e53399.

Petersen, C. I., Jheon, A. H., Mostowfi, P., Charles, C., Ching, S., Thirumangalathu, S., Barlow, L. A. and Klein, O. D. (2011). FGF signaling regulates the number of posterior taste papillae by controlling progenitor field size. *PLoS Genet.* **7**, e1002098.

Pézeron, G., Mourrain, P., Courty, S., Ghislain, J., Becker, T. S., Rosa, F. M. and David, N. B. (2008). Live analysis of endodermal layer formation identifies random walk as a novel gastrulation movement. *Curr. Biol.* **18**, 276-281.

Pogoda, H.-M., von der Hardt, S., Herzog, W., Kramer, C., Schwarz, H. and Hammerschmidt, M. (2006). The proneural gene ascl1a is required for endocrine differentiation and cell survival in the zebrafish adenohypophysis. *Development* **133**, 1079-1089.

Potel, M. J. and Mackay, S. A. (1979). Preaggregative cell motion in Dictyostelium. *J. Cell Sci.* **36**, 281-309.

R-Development-Core-Team (2008). R: A language and environment for statistical computing.R Foundation for Statistical Computing, Vienna, Austria. ISBN 3-900051-07-0.

Reifers, F., Böhli, H., Walsh, E. C., Crossley, P. H., Stainier, D. Y. and Brand, M. (1998). Fgf8 is mutated in zebrafish acerebellar (ace) mutants and is required for maintenance of midbrain-hindbrain boundary development and somitogenesis. *Development* **125**, 2381-2395.

Ren, W., Lewandowski, B. C., Watson, J., Aihara, E., Iwatsuki, K., Bachmanov, A. A., Margolskee, R. F. and Jiang, P. (2014). Single Lgr5- or Lgr6-expressing taste stem/progenitor cells generate taste bud cells ex vivo. *Proc. Natl. Acad. Sci. USA* **111**, 16401-16406.

Renaud, O., Herbomel, P. and Kissa, K. (2011). Studying cell behavior in whole zebrafish embryos by confocal live imaging: application to hematopoietic stem cells. *Nat. Protoc.* **6**, 1897-1904.

Roper, S. D. (2013). Taste buds as peripheral chemosensory processors. *Semin. Cell Dev. Biol.* **24**, 71-79.

Rothova, M., Thompson, H., Lickert, H. and Tucker, A. S. (2012). Lineage tracing of the endoderm during oral development. *Dev. Dyn.* **241**, 1183-1191.

Ruthardt, N., Lamb, D. C. and Bräuchle, C. (2011). Single-particle tracking as a quantitative microscopy-based approach to unravel cell entry mechanisms of viruses and pharmaceutical nanoparticles. *Mol. Ther.* **19**, 1199-1211.

Saxton, M. J. and Jacobson, K. (1997). Single-particle tracking: Applications to membrane dynamics. *Annu. Rev. Biophys. Biomol. Struct.* **26**, 373-399.

Seta, Y., Oda, M., Kataoka, S., Toyono, T. and Toyoshima, K. (2011). Mash1 is required for the differentiation of AADC-positive type III cells in mouse taste buds. *Dev. Dyn.* **240**, 775-784.

Spitzer, N. C. (2006). Electrical activity in early neuronal development. *Nature* **444**, 707-712.

Stone, L. M., Tan, S.-S., Tam, P. P. L. and Finger, T. E. (2002). Analysis of cell lineage relationships in taste buds. *J. Neurosci.* **22**, 4522-4529.

Sumen, C., Mempel, T. R., Mazo, I. B. and von Andrian, U. H. (2004). Intravital microscopy: visualizing immunity in context. *Immunity* **21**, 315-329.

Taruno, A., Vingtdeux, V., Ohmoto, M., Ma, Z., Dvoryanchikov, G., Li, A., Adrien, L., Zhao, H., Leung, S., Abernethy, M. et al. (2013). CALHM1 ion channel mediates purinergic neurotransmission of sweet, bitter and umami tastes. *Nature* **495**, 223-226.

Thirumangalathu, S., Harlow, D. E., Driskell, A. L., Krimm, R. F. and Barlow, L. A. (2009). Fate mapping of mammalian embryonic taste bud progenitors. *Development* **136**, 1519-1528.

Vandenbeuch, A., Larson, E. D., Anderson, C. B., Smith, S. A., Ford, A. P., Finger, T. E. and Kinnamon, S. C. (2015). Postsynaptic P2X3-containing receptors in gustatory nerve fibres mediate responses to all taste qualities in mice. *J. Physiol.* **593**, 1113-1125.

Wernet, M. F., Perry, M. W. and Desplan, C. (2015). The evolutionary diversity of insect retinal mosaics: common design principles and emerging molecular logic. *Trends Genet.* **31**, 316-328.

Yarmolinsky, D. A., Zuker, C. S. and Ryba, N. J. P. (2009). Common sense about taste: from mammals to insects. *Cell* **139**, 234-244.

Yee, K. K., Li, Y., Redding, K. M., Iwatsuki, K., Margolskee, R. F. and Jiang, P. (2013). Lgr5-EGFP marks taste bud stem/progenitor cells in posterior tongue. *Stem Cells* **31**, 992-1000.

Zhou, Y., Liu, H.-X. and Mistretta, C. M. (2006). Bone morphogenetic proteins and noggin: inhibiting and inducing fungiform taste papilla development. *Dev. Biol.* **297**, 198-213.

DEVELOPMENT